Applied Catalysis B: Environmental 201 (2017) 232–240

Contents lists available at ScienceDirect

Applied Catalysis B: Environmental

journal homepage: www.elsevier.com/locate/apcatb

Fe-g-C_3N_4/graphitized mesoporous carbon composite as an effective Fenton-like catalyst in a wide pH range

Jianqing Ma [a], Qunfeng Yang [a], Yuezhong Wen [a,b,*], Weiping Liu [a]

[a] Institute of Environmental Science, College of Environmental and Resource Sciences, Zhejiang University, Hangzhou 310058, China
[b] Zhejiang Provincial Key Laboratory of Organic Pollution Process and Control, Zhejiang University, Hangzhou 310058, China

ARTICLE INFO

Article history:
Received 6 April 2016
Received in revised form 11 August 2016
Accepted 20 August 2016
Available online 21 August 2016

Keywords:
Graphitic carbon nitride
Catalyst
Fenton-like reaction
Organic pollutant

ABSTRACT

Heterogeneous Fe-N complexes are a kind of promising catalysts for the Fenton-like reaction. The present study selected a stable and inexpensive g-C_3N_4 as the chelating agent and combined with the graphitized mesoporous carbon (GMC). The fabricated Fe-g-C_3N_4/GMC composite was characterized by several techniques including FTIR, XRD, XPS, TEM and STXM. Results showed clear sheets of g-C_3N_4 and graphite with Fe evenly distributed mostly in the Fe-N coordination form. The catalyst expressed high activity in the Fenton-like reaction in a wide pH range of 4–10. 99.2% removal of Acid Red 73 was obtained in 40 min, and the degradation data well fitted with the pseudo-first-order kinetics model. By correlating the constant of reaction rates calculated from the model and the Fe speciation contents of the samples prepared at different conditions, we deduced that Fe-N species are the most important active sites for the Fenton-like reaction. More importantly, hydroxyl radicals played a great role in the whole reaction yet their generation was independent of visible light. Cyclic voltammetry results confirmed that the GMC can accelerate the Fe(III)/Fe(II) redox cycle by enhancing electron transfer, and thus enable this Fenton-like catalyst to perform well in a wide pH range.

1. Introduction

Fenton reaction is a powerful and effective way to generate hydroxyl radical (•OH), one of the most potent oxidants known, and the last decades have seen its wide application in biological chemistry, organic synthesis and contaminant control [1,2]. However, Fenton reaction in wastewater treatment still suffers from shortcomings such as narrow pH range (near 3) and large amounts of iron precipitations [3–5]. Based on this, many researchers are enthusiastic about looking for efficient heterogeneous Fenton-like catalysts used in a wide pH range. The supported Fe-N complexes offer a promising solution to this problem. Ligands such as phthalocyanines [6] and tetraamido macrocyclic ligands [7] do not only stabilize the iron species, but also accelerate the Fe(III)/Fe(II) redox cycle thus resulting in the ability to work at higher pH values [8]. Nevertheless, these organic cheating ligands are usually unstable due to their self-oxidation and aggregation [9,10], which greatly limits their lifetime and practical applications.

Graphitic carbon nitride (g-C_3N_4) is a polymer with graphite-like structure, and in recent years tremendous attention has been paid in the field of photocatalysts due to its tunable electronic properties and excellent chemical stability [11–13]. In addition, g-C_3N_4 can be easily prepared through the polymerization of cheap precursors like urea [14], dicyandiamide [15], thiourea [16], cyanamide [12] and melamine [17]. Particularly, it contains so-called "nitrogen pots" with six nitrogen lone-pair electrons, which are ideal sites for the chemical modification [18]. It is reported that doping with metal atoms has successfully enhanced its activity mainly in photocatalytic processes and oxygen reduction reactions [19–21]. These nitrogen-metal macrocyclic materials, owing to their ligand-field effects and chemical stability, can also be promising candidates for the Fenton-like catalyst which can be used in a wide pH range.

The objective of this study is to explore the possibility of g-C_3N_4 being a vigorous Fenton-like catalyst. The combination of Fe doped g-C_3N_4 (Fe-g-C_3N_4) with the graphitized mesoporous carbon (GMC) resulted in efficient Fenton-like catalyst that worked in a wide pH range. The N-rich g-C_3N_4 can trap Fe atoms to form highly dispersed active sites. While GMC not only provide a mesoporous structure for the g-C_3N_4 sheet growth, but the similar sp^2 bonding structure on its surface promote the electron transfer through strong electronic coupling [20]. In particular, it is verified that the degradation was not dominated by the photocatalyzation like the

* Corresponding author at: Institute of Environmental Science, College of Environmental and Resource Sciences, Zhejiang University, Hangzhou 310058, China.
E-mail address: wenyuezhong@zju.edu.cn (Y. Wen).

http://dx.doi.org/10.1016/j.apcatb.2016.08.048
0926-3373/

studies reported before, indicating that Fe-g-C_3N_4/GMC composite would be a promising Fenton-like catalyst and further research will be carried out in the future.

2. Materials and methods

2.1. Materials

Graphitized Mesoporous Carbon (Aldrich Prod. No. 699624, nanopowder, <500 nm, >99.95%) was purchased from Sigma Aldrich Co., USA. $FeCl_3{\cdot}6H_2O$ (AR, 99.0%), dicyandiamide (CP, 98%) and hydrogen peroxide (GR, 30% w/w) and 2,2-Di-(4-hydrophenyl) propane (BPA) were obtained from National Medicines Corporation Ltd. of China. Acid Red 73 (AR 73) and Rhodamine B (Rh B) were purchased from Gracia Chemical Technology Co. Ltd. and Bodi Chemical Technology Co. Ltd. of China, respectively. *p*-Chlorophenol (4-CP) and 2,4,6-Trichlorophenol (2,4,6-TCP) were supplied by Aladdin industrial Corporation, China. Tetracycline hydrochloride (TCH) were obtained from Dr. Ehrenstorfer, GmbH, Germany. Relative Chemical structures of these organics are shown in Fig. S1. Other chemicals were of laboratory reagent grade and were used without further purification. The deionized water used in this study was produced using a UPK/UPT ultrapure water system.

2.2. Preparation of the catalysts

In a typical procedure, 1 g of dicyandiamide (DCD) was dissolved in 20 mL deionized water under 80 °C, and then 0.2027 g of $FeCl_3{\cdot}6H_2O$ was added to this solution and stirred for 1 h, followed by the addition of 0.1 g GMC. The mixture was continually stirred at 120 °C until water was completely evaporated. The dried mixture was grinded and heated to 600 °C in a nitrogen atmosphere with a rate of 10 °C/min and kept for 3 h. The obtained product was denoted as Fe-g-C_3N_4/GMC. g-C_3N_4 and Fe-g-C_3N_4 were also prepared by the same procedure with the precursors of DCD and DCD/$FeCl_3{\cdot}6H_2O$, respectively. Besides, other samples prepared with different $FeCl_3{\cdot}6H_2O$ dosage and heat temperature were also tested for reference. They were denoted as 600-1, 600-2, 600-4, 550-3, 650-3 and 700-3, and their detailed preparing conditions have been listed in Table S1. It should be noted that Fe-g-C_3N_4/GMC mentioned above was also abbreviated as 600-3.

2.3. Characterization methods

N_2 adsorption and desorption isotherms were obtained at 77 K on a NOVA2000e surface area & pore size analyzer (Quantachrome, USA), and pore size was determined by the BJH (Barret-Joyner-Hallender) method. The surface structure and morphology of the catalysts were characterized by a SIRON 200 Scanning Electron Microscope (SEM, FEI, USA), a Jem1200 Transmission electron Microscope (TEM, JEOL, Japan) and a Tecnai G2 F20 S High resolution Transmission electron Microscope (HRTEM, FEI, USA). Zeta potential (ZP) was measured by Malvern Nano-Z Zetasizer (ZET-3000HS, UK).

Fourier Transform Infrared Spectroscopy (FTIR) of the KBr pelleted samples were recorded on AVATAR 370 FTIR spectrometer (Thermo Nicolet, USA) over the wavenumber range 400–4000 cm^{-1}. X-ray diffraction (XRD) spectra were collected on a XRD-6000 X-ray diffractometer (Shimadzu, Japan) with a Cu Kα radiation (λ = 1.5406 Å) over a 2θ range of 10–60°. X-ray photoelectron spectroscopy (XPS) was collected on a K-alpha X-ray photoelectron spectrometer (Thermo Fisher Scientific, USA) with a monochromatic Al Kα source (1486.6 eV). All binding energies were referenced to the C 1s peak at 284.2 eV.

Scanning Transmission X-ray Microscope (STXM) was conducted at the beam line 08U1 of the Shanghai Synchrotron Radiation Facility (Shanghai, China). The photon energies of each element were adjusted just below or above the absorption edge, and were 706.6 eV and 702.0 eV for Fe, 399.2 eV and 397.6 eV for N, 530.8 eV and 528.6 eV for O. All the data were processed by the Dual Energy Element Distribution Software.

2.4. Performance tests of the catalysts

The degradation reaction was started with H_2O_2 concentration of 40 mM, a catalyst dosage of 0.8 g/L and an initial AR 73 concentration of 50 ppm without any pH adjustment (pH = 6.86). Specifically, dynamic experiments were performed in 250 mL beaker flasks, which were sealed and stirred with a speed of 150 rpm at room temperature. At desired intervals, proper solution was taken out and went through a 0.22 μm filter immediately to monitor the concentration by using UV-2410 UV–vis spectrometer (Shimadzu, Japan) at 508.5 nm. The data was fitted with the pseudo-first-order kinetic model, which is described by Eq. (1):

$$C = C_0 e^{-kt} \quad (1)$$

Where C_0 and C (mg/L) stands for the concentration at initial and time t, and k (min^{-1}) is the rate constant of this reaction. After 40 min, the mixture were centrifuged at 7000 rpm for 5 min. The sediment was dried at 60 °C and reused, while the supernate was treated according to literature [22] and analyzed by GC–MS (Agilent 7890-5975C instrument equipped with a HP-5 capillary column). Concentration of H_2O_2 in the solution was measured by spectrophotometric determination using titanium sulfate at 400 nm. The concentration of Rh B was also measured by the UV–vis spectrometer at 553 nm, while other four organics were analyzed by a Waters® e2695 reverse-phase HPLC coupled with a Waters® 2998 photodiode array detector (Milford, MA, USA). Analytical methods are expatiated in Table S2. As for the study of pH influence, HCl and NaOH solutions were employed to adjust the initial pH. Total Organic Carbon (TOC) was determined by a Multi N/C 3100 TOC analyzer (JENA, Germany) and the leaching of iron ions were measured by an AA800 atomic absorption spectrophotometer (PerkinElmer, USA).

Electron spin resonance (ESR) signals of the radicals trapped by DMPO were obtained on a BRUKER A300 electron paramagnetic resonance spectrometer. The settings were center field 3514.3 G, microwave frequency 9.85 GHz and power 20.27 mW.

Cyclic Voltammetry Measurements was carried out in a three electrode system, including a saturated calomel reference electrode (SCE), a platinum auxiliary electrode and a glassy carbon disk electrode (GCE, 3 mm). The catalyst was mixed with nafion and ethanol and painted on the surface of GCE. Cyclic voltammograms were recorded at a scan rate of 50 mV/s from 0.1 to 0.9 V in a 50 mg/L AR 73 solution containing 0.1 M KCl. Before measurement, this solution was purged with N_2 for 30 min to remove dissolved O_2.

3. Results and discussion

3.1. Morphology and structure of the catalyst

Pure g-C_3N_4 layers are firmly stacked and thereby it suffers from a small specific surface area [23]. In our study it is only 11.0 m^2/g. However, when doped with iron and coated on GMC, the specific surface area increased dramatically to 370.5 m^2/g, which is much higher than Fe-g-C_3N_4 (263.6 m^2/g) and GMC (82.2 m^2/g) (Table 1). The average pore diameter decreased after the modification but this decrease was not very prominent, while the pore volume increased greatly, suggesting Fe-g-C_3N_4/GMC is not the simple physical mixture of Fe-g-C_3N_4 and GMC. It is noted that Fe-g-C_3N_4 shows a porous morphology with an intersect channels structure (Fig. 1b) similar to a carbonaceous material reported

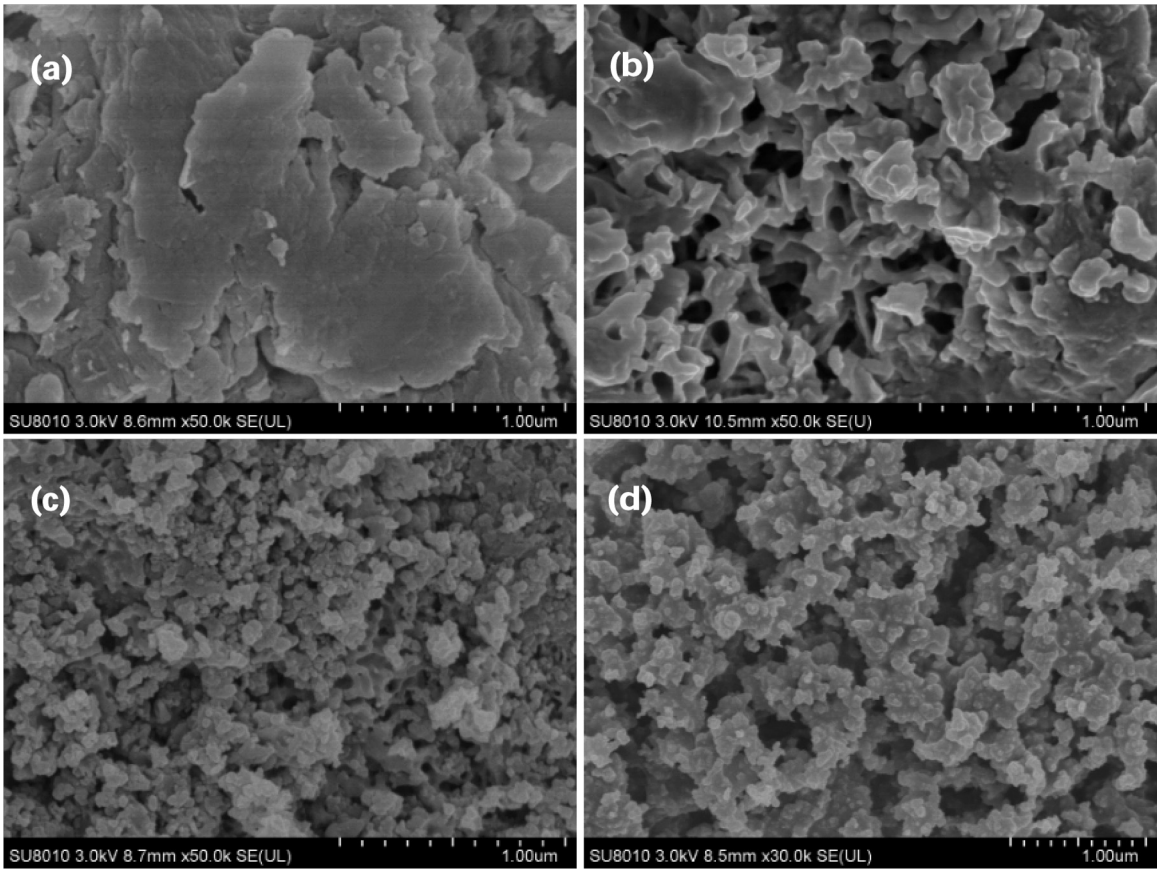

Fig. 1. TEM images of (a) g-C_3N_4, (b) Fe-g-C_3N_4, (c) Fe-g-C_3N_4/GMC and (d) GMC.

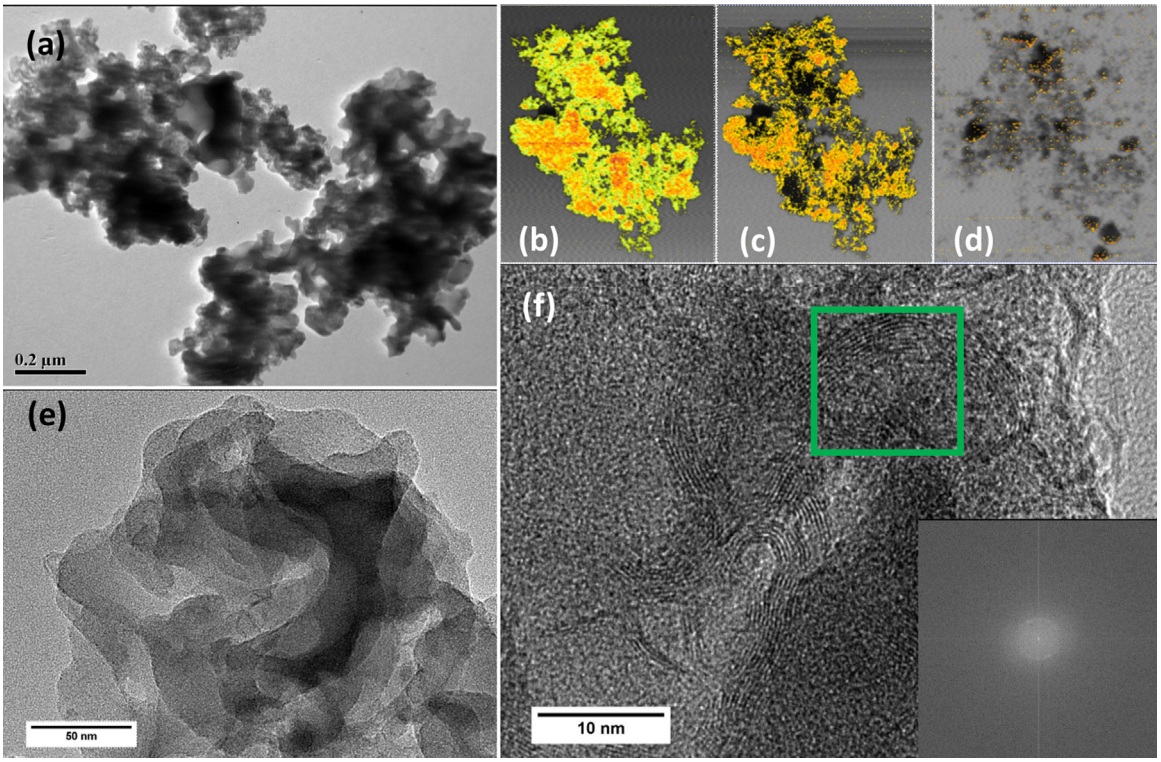

Fig. 2. Micrographs of Fe-g-C_3N_4/GMC, (a) TEM, (b–d) STXM element distribution of Fe, N and O, (e)–(f) HRTEM and the insert is FFT of the chosen area by the green box. (For interpretation of the references to colour in this figure legend, the reader is referred to the web version of this article.)

Table 1
Structure parameters of the four samples.

Samples	Specific Surface area (m^2/g)	Pore diameter (nm)	Pore volume (cc/g)
Fe-g-C_3N_4/GMC	370.5	3.006	0.569
g-C_3N_4	11.0	3.049	0.094
Fe-g-C_3N_4	263.6	3.015	0.268
GMC	82.2	3.030	0.261

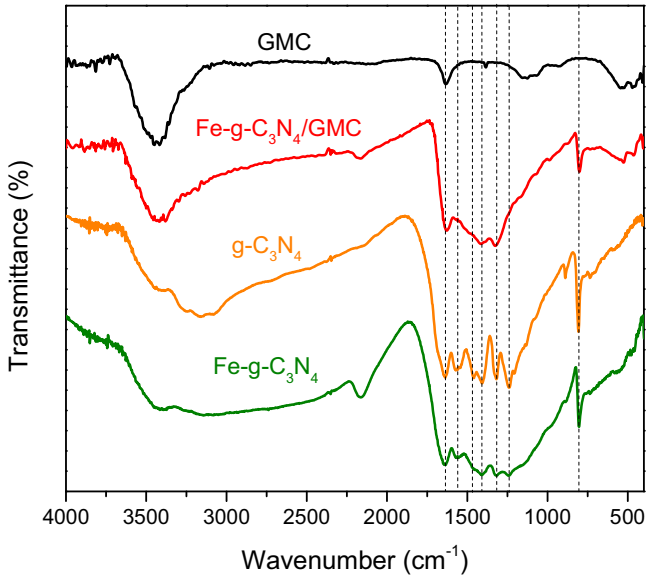

Fig. 3. FTIR spectra of Fe-g-C_3N_4/GMC, Fe-g-C_3N_4, g-C_3N_4 and GMC.

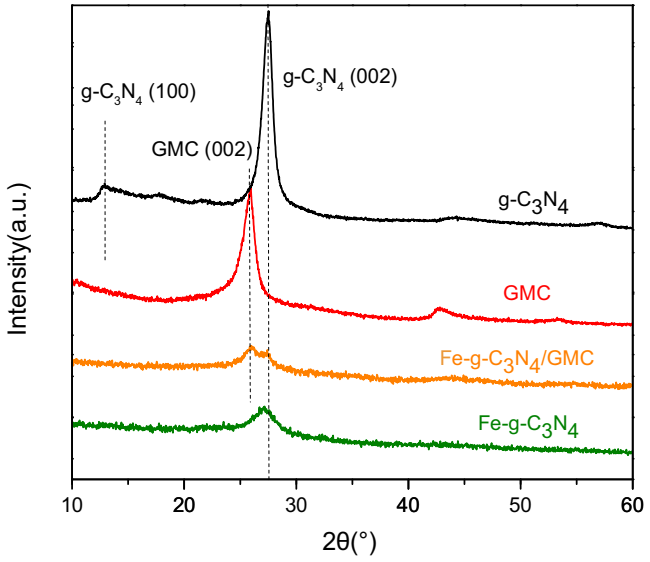

Fig. 4. XRD spectra of Fe-g-C_3N_4/GMC, Fe-g-C_3N_4, g-C_3N_4 and GMC.

in our earlier study [24], which is caused by the release of gases produced during the heating process. Most likely the addition of Fe induced part of the precursors decomposed at high temperature and consequently a great increase in the specific surface area. By contrast, Fe-g-C_3N_4/GMC displays a structure similar to GMC (Fig. 1c and d). And a typical IV isotherm with H3 hysteresis loop on Fe-g-C_3N_4/GMC isotherm was observed (Fig. S2), which means plate-like particles aggregated giving rise to slit-shaped pores [25]. These results further indicate a chemical interaction between Fe-g-C_3N_4 and the GMC surface thus inducing profound changes in morphology. Besides, Fe and N elements are almost homogeneously distributed (Fig. 2b–d) on the catalyst surface, and no visible particles or obvious crystallite structure can be attributed to Fe species in the HRTEM image (Fig. 2e and f).

FTIR spectra in Fig. 3 reveal that the inclusion of iron and GMC did little change to the basic C—N network. The typical breathing mode of the tris-*s*-triazine (806.5 cm^{-1}) and its stretching mode (1240–1640 cm^{-1}) are all found on the spectra of g-C_3N_4, Fe-g-C_3N_4 and Fe-g-C_3N_4/GMC. However, the band at 1242.0 cm^{-1} corresponded to the stretching vibration of C—NH—C (partial condensation) disappeared while the band at 1320.2 which is attributed to C—N(—C)—C (full condensation) remained only in the case of Fe-g-C_3N_4/GMC [26]. Clearly, the introduction of GMC results in strong condensation of g-C_3N_4, which is also supported by the stretching vibration modes of the weaker band around 3159 cm^{-1} for hydrogen-bonding interactions. The XRD patterns in Fig. 4 illustrate both g-C_3N_4 and GMC have a graphitic-like structure. Strong and sharp diffraction peaks at 27.6 and 25.37° are due to the stacking of the conjugated aromatic systems, indicating tight packing and strong binding between layers [20]. And their (002) interplanar distances for g-C_3N_4 and GMC are 0.323 and 0.351 nm, respectively [18]. Besides, another peak of g-C_3N_4 at 12.89° is ascribed to the (100) inplanar ordering of tri-s-triazine units with a period of 0.686 nm. After incorporation of iron and GMC, this peak disappeared and is the evidence for successful modification. In addition, the intensity of another two (002) peaks at 27.32 and 25.93° decreased dramatically, which means a rigid layer pack is inexistent. From this point of view, the disorder of the layer can be an explanation for their increase in specific surface area. Interestingly, no obvious Fe species peaks are observed, together with the absence of the (100) peak suggesting that the majority of Fe are present in an amorphous form, most likely in the form of Fe-N bonds rather than forming oxides or carbides [21], which is consistent with the HRTEM results discussed above. Future work will focus on its fine description of the coordination structure.

XPS analysis was used to explore the surface chemical state of the catalyst. It reveals that only four elements (C↘O↘N and Fe) are existed on the near surface. Fig. 5 depicts N1s and Fe 2p spectra recorded with Fe-g-C_3N_4/GMC. The peaks in N 1s are divided into for species: pyridinic N at 397.6 eV, N in triazine rings (C—N—C) at 398.6 eV, tertiary N (N-$(C)_3$) at 400.0 eV and oxidized N at 404.5 eV. Actually, the BE value of N coordinated with Fe (N-Fe) also lies in 398.8 ± 0.5 eV [20,27,28], which is too close to be distinguished from the C—N—C units. Herein pyridinic N, C—N—C/N-Fe are dominated species, which account for 42.7% and 44.2% of the total N. It is noteworthy that pydidinic N is ascribed to the nitrogen-carbon support interaction, which may serve as bridges linking carbon nitride polymers and carbon sheets [18]. The spectra of Fe 2p is deconvoluted into three major components, Fe bonded with nitrogen at 709.2 eV (45.5%), FeO/Fe_3O_4 at 710.4 eV (19.7%) and Fe_2O_3 at 711.5 eV (24.7%), no metallic Fe is found in this catalyst.

3.2. Catalytic and use performance

The catalytic performance was tested by AR 73, which belongs to the largest and the most important group of dyes [4]. As can be seen from Fig. 6a, the removal rates of AR73 by g-C_3N_4 and Fe-g-C_3N_4 were merely 3.45 and 29.7% in 40 min. While for Fe-g-C_3N_4/GMC,

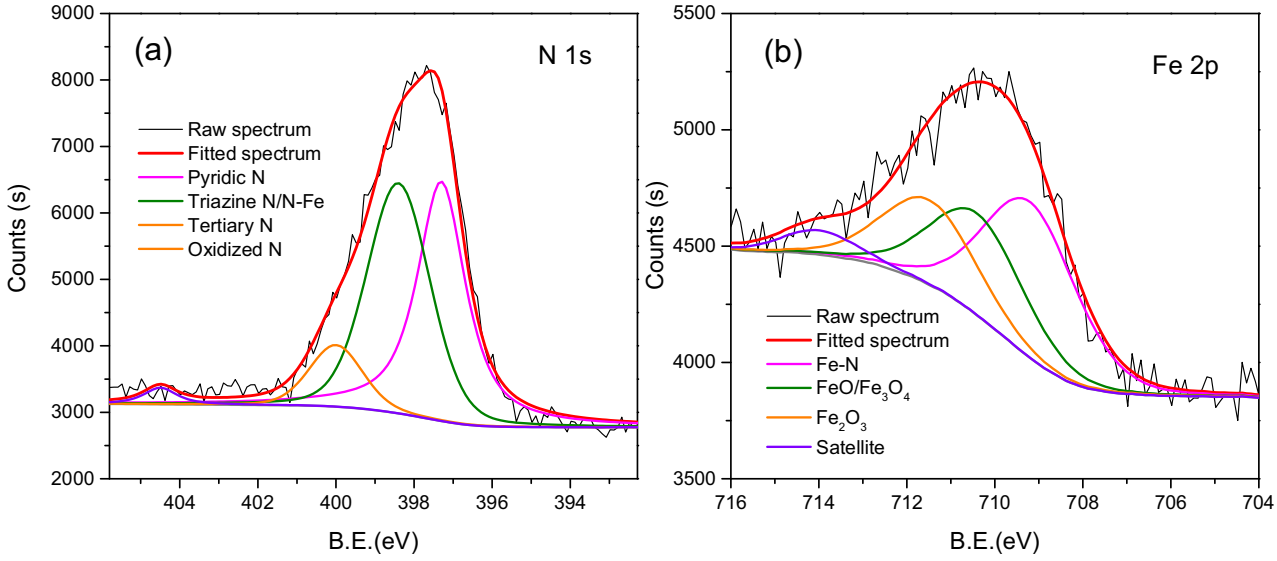

Fig. 5. XPS spectra and their deconvolution profiles of (a) N 1s and (b) Fe 2p spectra of Fe-g-C_3N_4/GMC.

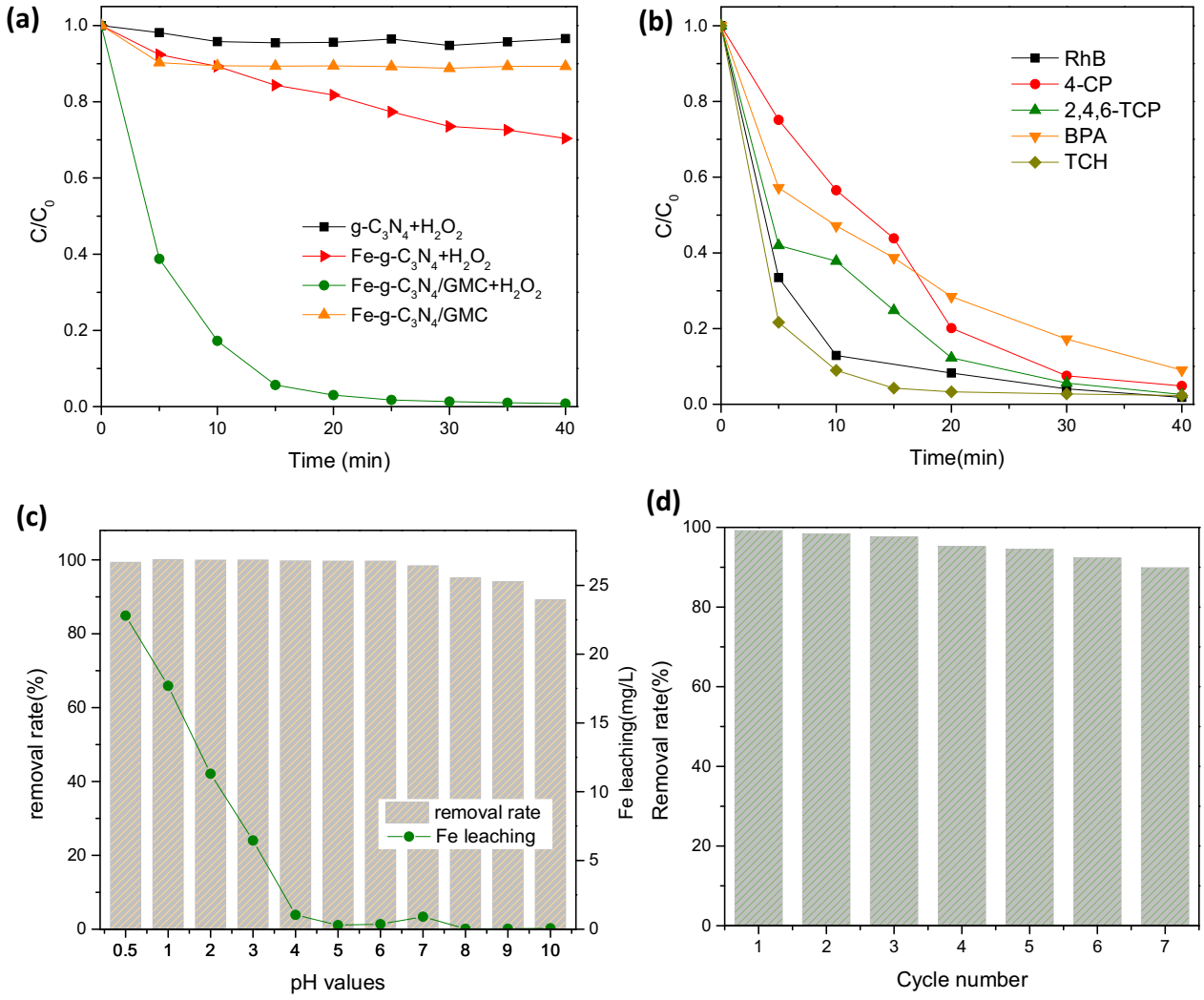

Fig. 6. Catalytic and use performances of Fe-g-C_3N_4/GMC. Unless specific state, the conditions are, AR73 with no pH adjustment 50 mg/L, catalyst 0.8 g/L, H_2O_2 40 mM, 40 min, 25 °C. (a) Time profiles of the AR 73 removal, and the adsorption without no H_2O_2 addition, the degradation by Fe-g-C_3N_4, g-C_3N_4 were also tested for reference. (b) Time profiles of other organics removal (BPA 20 mg/L, the rest 50 mg/L). (c) Effect of pH values on the AR 73 removal and Fe leaching. (d) 7 cycles of reuse test.

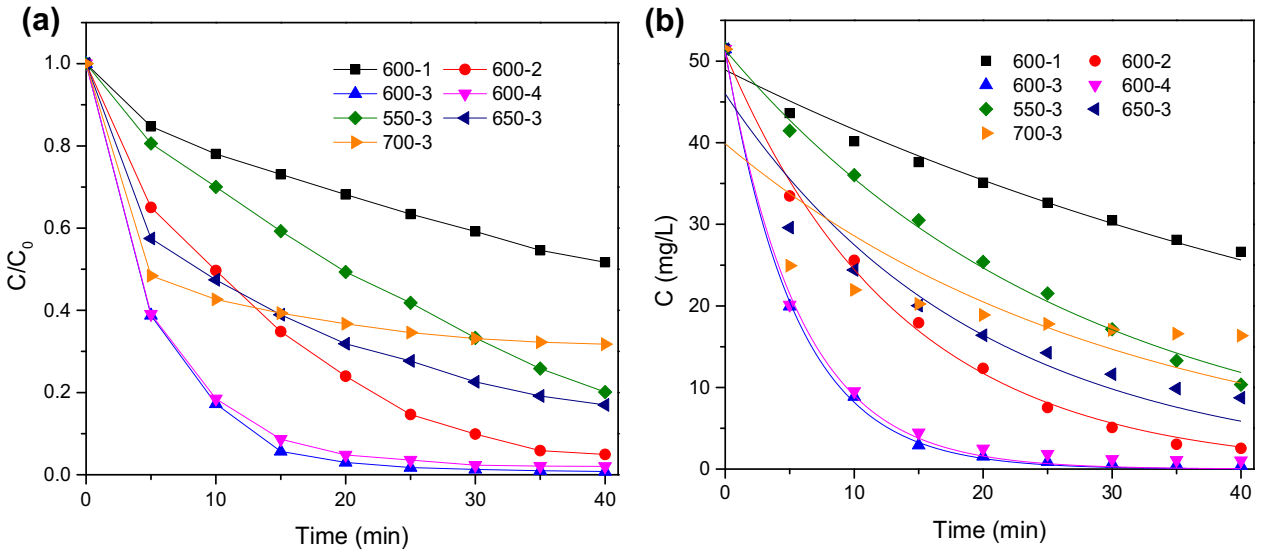

Fig. 7. (a)Time profiles of the AR 73 removal by catalysts prepared at different conditions (AR 73 50 mg/L, 100 mL, catalyst 0.8 g/L, H_2O_2 40 mM) and (b) its pseudo-first-order kinetic model fitting curves.

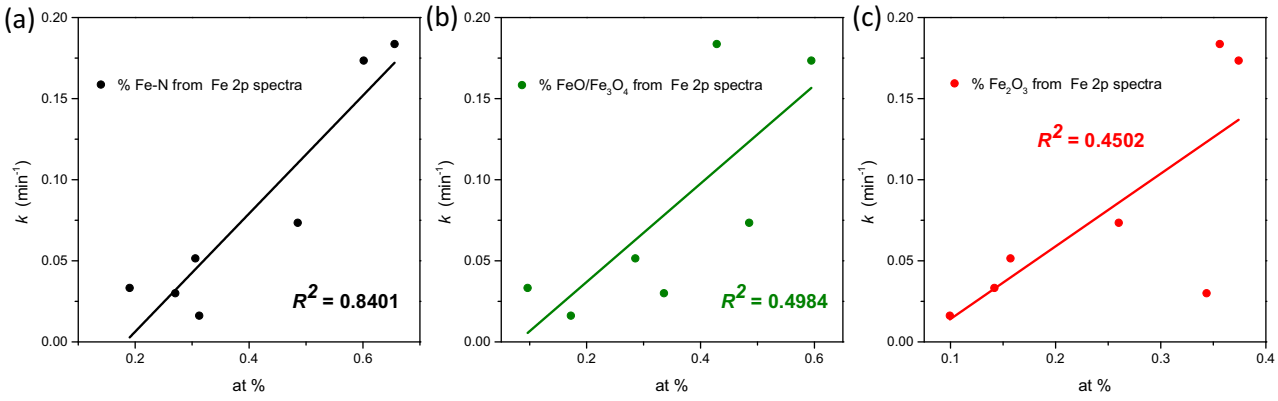

Fig. 8. Linear fit of rate constants from kinetic models and the atomic percentage of (a) Fe-N centers, (b) FeO/Fe_3O_4, (c) Fe_2O_3 calculated from Fe 2p spectra.

Table 2
N and Fe speciation (at.%) from XPS analysis for samples prepared at different conditions.

Samples	Pyridnic N	N-Fe	Pyrrolic N	Oxidized N	Total N	Metallic Fe	Fe-N	FeO/Fe_3O_4	Fe_2O_3	Total Fe
600-1	16.68	7.10	1.27	0.27	25.31	0.07	0.31	0.17	0.10	0.65
600-2	9.69	7.33	3.60	0.22	20.84	0.09	0.49	0.47	0.26	1.21
600-3	6.36	6.59	1.68	0.26	14.89	/	0.66	0.43	0.36	1.44
600-4	4.30	7.78	2.10	0.21	14.39	/	0.60	0.59	0.37	1.57
550-3	3.50	3.99	3.42	/	10.91	/	0.27	0.34	0.34	0.95
650-3	1.50	2.83	1.07	0.42	5.82	0.06	0.31	0.29	0.16	0.81
700-3	0.77	0.19	0.19	0.16	1.31	0.07	0.19	0.10	0.14	0.50

this removal rate reached up to 99.2% (94.3% in the first 15 min). As reference, the adsorption efficiency was only 10.7% when H_2O_2 was absent, suggesting the whole removal process was dominated by the degradation. The total organic carbon (TOC) removal was about 42.9%. GC–MS analysis after trimethylsiylation by BSTFA revealed that main products were cinnamic acid, propionic acid, 1-nitro-2-naphthol and acetic acid, indicating the cleavage of the azo bond and an increase in biodegradability.

The adaptability of the catalyst to different kinds of pollutants and pH values was further examined. Fig. 6b shows that over 91% of all organics, including Rhodamine B (Rh B), *p*-Chlorophenol (4-CP), 2,4,6-trichlorophenol (2,4,6-TCP), bisphenol A (BPA) and tetracycline hydrochloride (TCH), were removed in 40 min. Adsorption experiments showed less than 13% of these organics could be removed without the help of H_2O_2 (Fig. S6). Fig. 6c indicates that Fe-g-C_3N_4/GMC performed well in a wide pH range. However, at strong acidic conditions the leaching Fe contents were higher than the limitation in EU and US (<2 ppm) [29], so Fe-g-C_3N_4/GMC is recommended in the pH range of 4–10. When pH=4 the Fe leaching was 1.04 ppm, while at the same concentration, the removal rates of homogeneous Fenton reaction triggered by Fe^{2+} and Fe^{3+} (in their hydrochloride form) were 29.7% and 13.4%, much lower than that of Fe-g-C_3N_4/GMC. It is believed that the leaching Fe makes fairly limited contribution to the AR 73 removal.

The reusability is one of the major issues to evaluate a catalyst's performance [30]. In the present study, Fe-g-C_3N_4/GMC were tested for seven cycles. And in this process the ability to remove AR 73 slightly decreased (Fig. 6d). It was found that the morphology

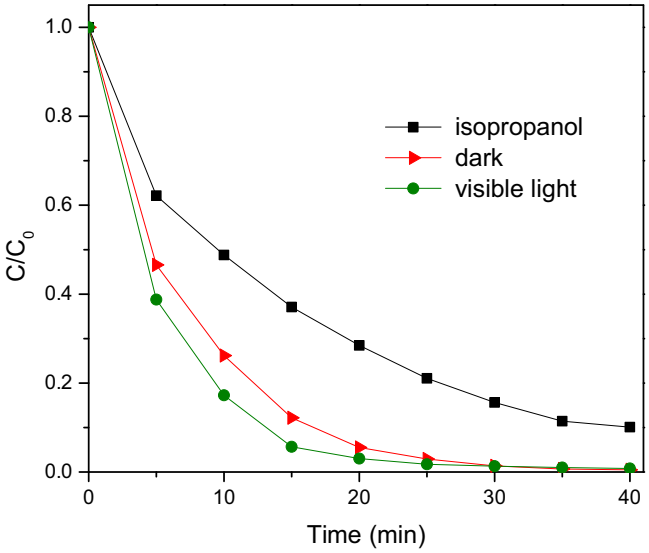

Fig. 9. Time profiles of the AR 73 removal by Fe-g-C_3N_4/GMC at dark and 0.3 M isopropanol.

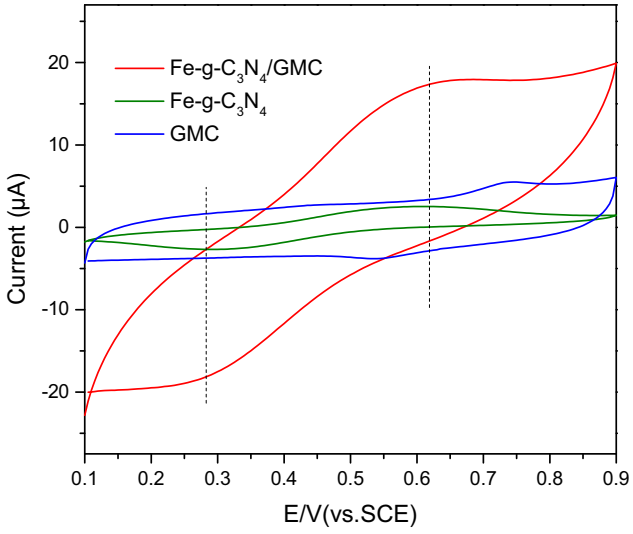

Fig. 11. Cyclic voltammogram (CV) scan of catalysts coated GCE electrode in a solution containing 50 mg/L AR 73 and 0.1 M KCl.

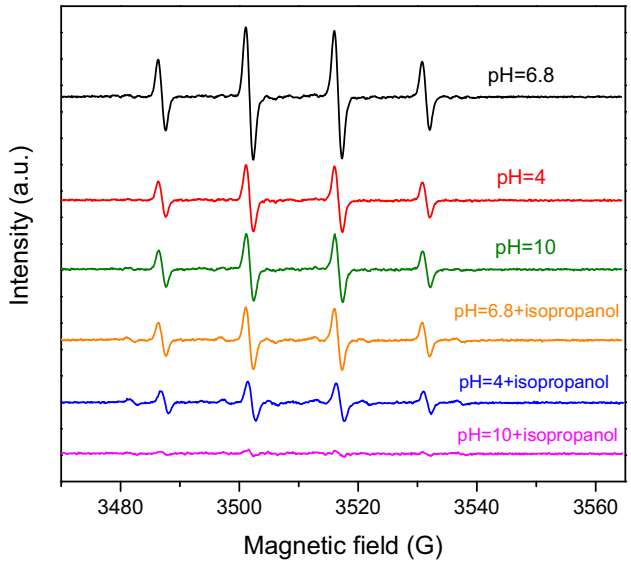

Fig. 10. DMPO spin-trapping ESR spectra of ·OH radicals with or without the addition of 0.3 M isopropanol at different pH values (AR 73 50 mg/L, catalyst 0.8 g/L, H_2O_2 40 mM). The samples were taken out at the 5 min and immediately added 0.18 M DMPO.

of the used catalyst was almost unchanged (Fig. S9a). Tiny particles with several nm emerged at the brink of the catalyst, which may be responsible for the decline of AR73 removal. The HRTEM image shows a clear monocrystalline structure and an interplanar spacing of 0.27 nm, which is assigned to the (104) planes of α-Fe_2O_3 (Fig. S9b) and probably generated in the Fenton-like reaction or the heating treatment. More work should be done to uncover the reason of these particle's emergence and further enhance the reuse stability of the catalyst.

3.3. Catalytic active sites

In order to explore the catalytic actives sites, we prepared several catalysts with different amounts of Fe addition and heating temperature. Clearly, preparation conditions can exert great impact on the catalysts surface state, which can be directly examined through the morphological studies (Fig. S3) and the removal ability of AR 73. It is shown from Fig. 7 that with the increase of Fe, the degradation ability reached a maximum (Fe-g-C_3N_4/GMC) and then slightly decreased, which means total Fe is not the only influential factor for the catalyst. Fig. S7 shows the adsorption contributed little to the AR 73 removal by 600-1, 600-2, 600-3 and 600-4. Therefore, their difference in the AR 73 removal mainly results from the oxidation, that is to say, the catalytic ability of producing •OH. An acceptable explanation is that excess of Fe in 600-4 would increase inactive species in the catalyst, thus more H_2O_2 was decomposed to O_2 rather than •OH. And this is partially proved by its rapid consumption of H_2O_2 in Fig. S8. On the other hand, higher temperature accelerated the decomposition of the Fe-g-C_3N_4 network, which was verified by the FTIR and XRD analysis (Fig. S4 and S5). According to the XPS results (Table 2), a dramatic decline of the surface Fe content of the samples prepared at 650 and 700 °C was found, while their bulk contents were still high (Table S1). This phenomenon can be interpreted by the formation of metallic iron and carbide as well as their imbedding into the carbon layers [31]. Consequently, the potential active sites on the catalysts surface decreased, resulting in poor ability to degrade the dye AR 73.

The next move was to figure out which species made up these active sites. Firstly, the degradation process of all catalysts was fitted by the pseudo-first-order kinetic model, and corresponding parameters are listed in Table 3. From the correlation coefficient point of view, this model describes well for most catalysts. However, the sample prepared at 700 °C had a strong adsorption for AR 73 and thus made the whole removal process complicated and did not fit the model. Secondly, an in-depth correlation between surface chemistry data obtained from XPS analysis and activity (degradation rate constant k from fitted kinetic model) was done. It is shown from Fig. 8 that the catalytic activity showed high correlation in the presence of Fe-N species ($R^2 = 0.84$), while low correlation with the amounts of FeO/Fe_3O_4 and Fe_2O_3 ($R^2 < 0.50$). The best performing sample of Fe-g-C_3N_4/GMC also has the largest amount of Fe-N centers. It can be concluded that Fe-N centers are the main active sites for the Fenton-like reaction. The correlation between rate constants and the specific surface area were also calculated (Fig. S11, $R^2 = 0.0294$), which suggested that this catalytic reaction relies heavily on the amount of surface active species rather than the specific surface area.

Table 3
Parameters of the pseudo-first-order kinetic models of different catalysts.

Parameters	600-1	600-2	600-3	600-4	550-3	650-3	700-3
k	0.0162	0.0734	0.1837	0.1734	0.0367	0.0515	0.0333
R^2	0.9715	0.9960	0.9991	0.9961	0.9945	0.9242	0.6157

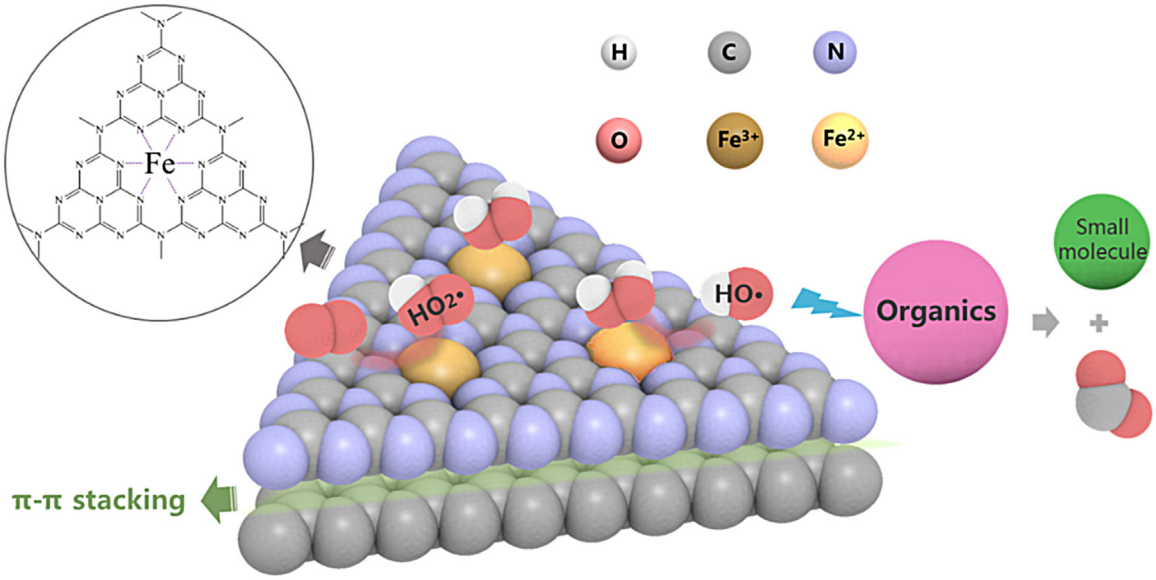

Fig. 12. Schematic diagram of Fe-g-C_3N_4/GMC catalyzed Fenton-like reaction.

3.4. Proposed mechanisms

In many cases, g-C_3N_4 and its derivatives are used as photocatalysts [12,15,16,21]. So whether the degradation is light-dependent or not needs to be examined. The experiment was conducted in dark while other conditions were unchanged. At initial stage there was very less difference (~8%) of dye removal rate between dark and visible light. As time interval increased, the difference gradually decreased and eventually disappeared at about 30 min (Fig. 9). This result illustrates that light plays almost no role in the degradation process, which is different from the photo-induced mechanism reported before.

In order to have deeper insight into the reaction paths, we examined the major active oxygen species involved in the degradation of AR 73. Herein we chose isopropanol as the hydroxyl radical scavenger [32]. Once added the removal rate of AR 73 was suppressed but not too much, suggesting the •OH took part in the oxidation process. ESR technique further confirmed the existence of this oxygen species. The ESR spectra in Fig. 10 displayed a typical 4-fold peak with an intensity ratio of 1:2:2:1, which can be ascribed to the DMPO-·OH [33]. It should be noted that even after the addition of isopropanol, this peak can be detected still. From this we deduced that the only 10% suppress of removal rate can be possibly explained by the adsorption/surface-oxidation mechanism [34–36]. The affinity of AR 73 to Fe-g-C_3N_4/GMC was stronger than that of isopropanol, resulting in the accumulation of AR 73 rather than isopropanol around, and then the Fenton-like reaction occurred on the catalyst surface. It was found that Fe-g-C_3N_4/GMC had negative surface-charge from pH value 5–10 according to the zeta potential tests (Fig. S10), therefore it was difficult to attract AR 73 in anionic ions form [37] by electrostatic interactions. Due to the existence of graphitic-like structure in Fe-g-C_3N_4/GMC and aromatic rings in AR 73, it is reasonable to ascribe this stronger affinity to π-π interaction.

The higher efficiency at a wide pH range observed by Fe-g-C_3N_4/GMC may be due to (i) the complexation of iron by g-C_3N_4, not only leading to a soluble and reactive form of iron at different pH values, but also the advantageously modification of the redox properties by ligand-field effects [38], (ii) the cooperation with GMC through π-π stacking similar to the illustration of graphene [20,39,40], accelerating electron transfer in the Fe(III)/Fe(II) cycles and attracting organics to the catalyst surface. A cyclic voltammetry test was performed to support our view. A reduction peak at about 0.3 V was observed both in Fe-g-C_3N_4/GMC and Fe-g-C_3N_4, but Fe-g-C_3N_4/GMC possessed much higher reduction current (Fig. 11), which indicated faster electron transfer from Fe(III)/Fe(II) reduction.

By combining all the results and discussion above, we proposed a possible mechanism of the Fenton-like reaction catalyzed by Fe-g-C_3N_4/GMC (Fig. 12). The reaction starts with the formation of a precursory surface complex by H_2O_2 and Fe(III)-N. Then the complex decomposes to Fe(II)-N and HO· by a reversible electron transfer, triggering a series of chain reaction involving the formation of ·OH and the redox cycle of Fe(III)/Fe(II) [41]. In fact, this step is the rate-limiting step of the whole reaction, as its rate constants is only 2.5×10^{-3} M^{-1} s^{-1}, much lower than other steps [42]. Nevertheless, it is facilitated with the Fe-N ligands and further the π-π stacking with GMC, thus creates an excellent catalytic ability of Fe-g-C_3N_4/GMC. At the same time, hydroxyl radicals mainly attack organics adsorbed on the near-surface of the catalyst, avoiding the effect of HO^- and other possible scavengers from the bulk solution.

4. Conclusions

In this study, a Fe doped g-C_3N_4 combined with graphitized mesoporous carbon composite was fabricated and used as a vigorous Fenton-like catalyst. This Fe-g-C_3N_4/GMC shows an excellent performance for the degradation of AR 73 in a pH range of 4–10, as well as acceptable usability and wide adaptation for other organic

pollutants. Fe is evenly distributed on the g-C_3N_4 network, and those that coordinated with N are the major active sites. The action is dominated by ·OH yet its generation is independent of the visible light. Finally, graphitized mesoporous carbon provides a porous structure and an enhancement in electron transfer for the Fe(III)/Fe(II) redox cycle, which creates high efficiency in Fenton-like reaction.

Acknowledgements

The authors acknowledge financial support from 863 Research Project (2013AA065202) and Science and Technology Department of Jinhua Municipality (grant No. 2015-3-054). We also thank the staff at beamlines BL08U at the Shanghai Synchrotron Radiation Facility (SSRF) for providing the beam time and data analysis.

Appendix A. Supplementary data

Supplementary data associated with this article can be found, in the online version, at http://dx.doi.org/10.1016/j.apcatb.2016.08.048.

References

[1] J.J. Pignatello, E. Oliveros, A. MacKay, Advanced oxidation processes for organic contaminant destruction based on the Fenton reaction and related chemistry, Crit. Rev. Environ. Sci. Technol. 36 (2006) 1–84.
[2] J.L. Wang, L.J. Xu, Advanced oxidation processes for wastewater treatment: formation of hydroxyl radical and application, Crit. Rev. Environ. Sci. Technol. 42 (2012) 251–325.
[3] C.L. Hsueh, Y.H. Huang, C.C. Wang, C.-Y. Chen, Degradation of azo dyes using low iron concentration of Fenton and Fenton-like system, Chemosphere 58 (2005) 1409–1414.
[4] P.V. Nidheesh, R. Gandhimathi, S.T. Ramesh, Degradation of dyes from aqueous solution by Fenton processes: a review, Environ. Sci. Pollut. Res. 20 (2013) 2099–2132.
[5] W. Luo, L. Zhu, N. Wang, H. Tang, M. Cao, Y. She, Efficient removal of organic pollutants with magnetic nanoscaled BiFeO3 as a reusable heterogeneous Fenton-like catalyst, Environ. Sci. Technol. 44 (2010) 1786–1791.
[6] C. Shen, Y. Wen, Z. Shen, J. Wu, W. Liu, Facile, green encapsulation of cobalt tetrasulfophthalocyanine monomers in mesoporous silicas for the degradative hydrogen peroxide oxidation of azo dyes, J. Hazard. Mater. 193 (2011) 209–215.
[7] S.S. Gupta, M. Stadler, C.A. Noser, A. Ghosh, B. Steinhoff, D. Lenoir, C.P. Horwitz, K.-W. Schramm, T.J. Collins, Rapid total destruction of chlorophenols by activated hydrogen peroxide, Science 296 (2002) 326–328.
[8] B. Ensing, F. Buda, E.J. Baerends, Fenton-like chemistry in water: oxidation catalysis by Fe(III) and H_2O_2, J. Phys. Chem. A 107 (2003) 5722–5731.
[9] C. Lee, D.L. Sedlak, A novel homogeneous Fenton-like system with Fe(III)–phosphotungstate for oxidation of organic compounds at neutral pH values, J. Mol. Catal. A Chem. 311 (2009) 1–6.
[10] B. Agboola, K.I. Ozoemena, T. Nyokong, Hydrogen peroxide oxidation of 2-chlorophenol and 2,4,5-trichlorophenol catalyzed by monomeric and aggregated cobalt tetrasulfophthalocyanine, J. Mol. Catal. A: Chem. 227 (2005) 209–216.
[11] Z. Zhao, Y. Sun, F. Dong, Graphitic carbon nitride based nanocomposites: a review, Nanoscale 7 (2015) 15–37.
[12] X. Wang, K. Maeda, A. Thomas, K. Takanabe, G. Xin, J.M. Carlsson, K. Domen, M. Antonietti, A metal-free polymeric photocatalyst for hydrogen production from water under visible light, Nat. Mater. 8 (2009) 76–80.
[13] J. Zhu, P. Xiao, H. Li, S.A.C. Carabineiro, Graphitic carbon nitride: synthesis, properties, and applications in catalysis, ACS Appl. Mater. Interfaces 6 (2014) 16449–16465.
[14] L. Shi, L. Liang, F. Wang, M. Liu, K. Chen, K. Sun, N. Zhang, J. Sun, Higher yield urea-derived polymeric graphitic carbon nitride with mesoporous structure and superior visible-light-responsive activity, ACS Sustain. Chem. Eng. 3 (2015) 3412–3419.
[15] X. Chen, J. Zhang, X. Fu, M. Antonietti, X. Wang, Fe-g-C3N4-catalyzed oxidation of benzene to phenol using hydrogen peroxide and visible light, J. Am. Chem. Soc. 131 (2009) 11658–11659.
[16] G. Zhang, J. Zhang, M. Zhang, X. Wang, Polycondensation of thiourea into carbon nitride semiconductors as visible light photocatalysts, J. Mater. Chem. 22 (2012) 8083–8091.
[17] Y. Zhang, Q. Pan, G. Chai, M. Liang, G. Dong, Q. Zhang, J. Qiu, Synthesis and luminescence mechanism of multicolor-emitting g-C_3N_4 nanopowders by low temperature thermal condensation of melamine, Sci. Rep. Uk 3 (2013).
[18] M.-Q. Wang, W.-H. Yang, H.-H. Wang, C. Chen, Z.-Y. Zhou, S.-G. Sun, Pyrolyzed Fe-N-C composite as an efficient non-precious metal catalyst for oxygen reduction reaction in acidic medium, ACS Catal. 4 (2014) 3928–3936.
[19] X. Wang, X. Chen, A. Thomas, X. Fu, M. Antonietti, Metal-containing carbon nitride compounds: a new functional organic–metal hybrid material, Adv. Mater. 21 (2009) 1609–1612.
[20] Q. Liu, J. Zhang, Graphene supported Co-g-C_3N_4 as a novel metal–macrocyclic electrocatalyst for the oxygen reduction reaction in fuel cells, Langmuir 29 (2013) 3821–3828.
[21] Z. Li, C. Kong, G. Lu, Visible photocatalytic water splitting and photocatalytic two-electron oxygen formation over Cu-and Fe-doped g-C_3N_4, J. Phys. Chem. C 120 (2015) 56–63.
[22] L. Lyu, L. Zhang, Q. Wang, Y. Nie, C. Hu, Enhanced fenton catalytic efficiency of γ-Cu-Al_2O_3 by σ-Cu^{2+}-ligand complexes from aromatic pollutant degradation, Environ. Sci. Technol. 49 (2015) 8639–8647.
[23] S. Yang, Y. Gong, J. Zhang, L. Zhan, L. Ma, Z. Fang, R. Vajtai, X. Wang, P.M. Ajayan, Exfoliated graphitic carbon nitride nanosheets as efficient catalysts for hydrogen evolution under visible light, Adv. Mater. 25 (2013) 2452–2456.
[24] Y. Wen, J. Ma, J. Chen, C. Shen, H. Li, W. Liu, Carbonaceous sulfur-containing chitosan-Fe(III): a novel adsorbent for efficient removal of copper(II) from water, Chem. Eng. J. 259 (2015) 372–380.
[25] S. Guo, D. Li, L. Zhang, J. Li, E. Wang, Monodisperse mesoporous superparamagnetic single-crystal magnetite nanoparticles for drug delivery, Biomaterials 30 (2009) 1881–1889.
[26] J. Liu, T. Zhang, Z. Wang, G. Dawson, W. Chen, Simple pyrolysis of urea into graphitic carbon nitride with recyclable adsorption and photocatalytic activity, J. Mater. Chem. 21 (2011) 14398–14401.
[27] A. Serov, K. Artyushkova, P. Atanassov, Fe-N-C oxygen reduction fuel cell catalyst derived from carbendazim: synthesis, structure, and reactivity, Adv. Energy Mater. 4 (2014).
[28] L. Yu, Y. Shen, Y. Huang, N. Fe, C catalyst modified graphene sponge as a cathode material for lithium-oxygen battery, J. Alloy Compd. 595 (2014) 185–191.
[29] X. Li, X. Liu, L. Xu, Y. Wen, J. Ma, Z. Wu, Highly dispersed Pd/PdO/Fe_2O_3 nanoparticles in SBA-15 for Fenton-like processes: confinement and synergistic effects, Appl. Catal. B-Environ. 165 (2015) 79–86.
[30] W. Liu, J. Ma, C. Shen, Y. Wen, W. Liu, A pH-responsive and magnetically separable dynamic system for efficient removal of highly dilute antibiotics in water, Water Res. 90 (2016) 24–33.
[31] K.P. Singh, E.J. Bae, J.-S. Yu, P. Fe, A new class of electroactive catalyst for oxygen reduction reaction, J. Am. Chem. Soc. 137 (2015) 3165–3168.
[32] M. Mrowetz, E. Selli, Enhanced photocatalytic formation of hydroxyl radicals on fluorinated TiO_2, Phys. Chem. Chem. Phys. 7 (2005) 1100–1102.
[33] Z. Matuszak, K.J. Reszka, C.F. Chignell, Reaction of melatonin and related indoles with hydroxyl radicals: EPR and spin trapping investigations, Free Radic. Biol. Med. 23 (1997) 367–372.
[34] S.-T. Yang, W. Zhang, J. Xie, R. Liao, X. Zhang, B. Yu, R. Wu, X. Liu, H. Li, Z. Guo, Fe_3O_4@SiO_2 nanoparticles as a high-performance Fenton-like catalyst in a neutral environment, RSC Adv. 5 (2015) 5458–5463.
[35] J.I. Nieto-Juarez, K. Pierzchła, A. Sienkiewicz, T. Kohn, Inactivation of MS2 coliphage in Fenton and Fenton-like systems: role of transition metals, hydrogen peroxide and sunlight, Environ. Sci. Technol. 44 (2010) 3351–3356.
[36] S.-Y. Pang, J. Jiang, J. Ma, Oxidation of sulfoxides and arsenic(III) in corrosion of nanoscale zero valent iron by oxygen: evidence against ferryl ions (Fe(IV)) as active intermediates in Fenton reaction, Environ. Sci. Technol. 45 (2010) 307–312.
[37] H.P. De Oliveira, Determination of pK a of dyes by electrical impedance spectroscopy, Microchem. J. 88 (2008) 32–37.
[38] A. Georgi, A. Schierz, U. Trommler, C.P. Horwitz, T.J. Collins, F.D. Kopinke, Humic acid modified Fenton reagent for enhancement of the working pH range, Appl. Catal. B-Environ. 72 (2007) 26–36.
[39] S.-Q. Liu, B. Xiao, L.-R. Feng, S.-S. Zhou, Z.-G. Chen, C.-B. Liu, F. Chen, Z.-Y. Wu, N. Xu, W.-C. Oh, Graphene oxide enhances the Fenton-like photocatalytic activity of nickel ferrite for degradation of dyes under visible light irradiation, Carbon 64 (2013) 197–206.
[40] N.A. Zubir, C. Yacou, J. Motuzas, X. Zhang, J.C.D. da Costa, Structural and functional investigation of graphene oxide–Fe_3O_4 nanocomposites for the heterogeneous Fenton-like reaction, Sci. Rep. Uk 4 (2014).
[41] S.-S. Lin, M.D. Gurol, Catalytic decomposition of hydrogen peroxide on iron oxide: kinetics, mechanism, and implications, Environ. Sci. Technol. 32 (1998) 1417–1423.
[42] W.P. Kwan, B.M. Voelker, Decomposition of hydrogen peroxide and organic compounds in the presence of dissolved iron and ferrihydrite, Environ. Sci. Technol. 36 (2002) 1467–1476.